NANO LETTERS

Letter

pubs.acs.org/NanoLett

Synthesis of $WS_{2x}Se_{2-2x}$ Alloy Nanosheets with Composition-Tunable Electronic Properties

Xidong Duan,[#,⊗] Chen Wang,[‡,⊗] Zheng Fan,[‡] Guolin Hao,[⊥] Liangzhi Kou,[∥] Udayabagya Halim,[⊥] Honglai Li,[†] Xueping Wu,[†] Yicheng Wang,[†] Jianhui Jiang,[#] Anlian Pan,[#,†] Yu Huang,[‡,§] Ruqin Yu,[*,#,†] and Xiangfeng Duan[*,⊥,§]

[#]State Key Laboratory of Chemo/Biosensing and Chemometrics, College of Chemistry and Chemical Engineering, and [†]Key Laboratory for Micro-Nano Physics and Technology of Hunan Province, School of Physics and Electronics, Hunan University, Changsha, Hunan 410082, P. R. China

[‡]Department of Materials Science and Engineering, [⊥]Department of Chemistry and Biochemistry, and [§]California NanoSystems Institute, University of California, Los Angeles, California 90095, United States

[∥]School of Chemistry, Physics and Mechanical Engineering Faculty, Queensland University of Technology, Garden Point Campus, QLD 4001 Brisbane, Australia

Supporting Information

ABSTRACT: Two-dimensional (2D) layered transition metal dichalcogenides (TMDs) have recently emerged as a new class of atomically thin semiconductors for diverse electronic, optoelectronic, and valleytronic applications. To explore the full potential of these 2D semiconductors requires a precise control of their band gap and electronic properties, which represents a significant challenge in 2D material systems. Here we demonstrate a systematic control of the electronic properties of 2D-TMDs by creating mixed alloys of the intrinsically p-type WSe_2 and intrinsically n-type WS_2 with variable alloy compositions. We show that a series of $WS_{2x}Se_{2-2x}$ alloy nanosheets can be synthesized with fully tunable chemical compositions and optical properties. Electrical transport studies using back-gated field effect transistors demonstrate that charge carrier types and threshold voltages of the alloy nanosheet transistors can be systematically tuned by adjusting the alloy composition. A highly p-type behavior is observed in selenium-rich alloy, which gradually shifts to lightly p-type, and then switches to lightly n-type characteristics with the increasing sulfur atomic ratio, and eventually evolves into highly n-doped semiconductors in sulfur-rich alloys. The synthesis of $WS_{2x}Se_{2-2x}$ nanosheets with tunable optical and electronic properties represents a critical step toward rational design of 2D electronics with tailored spectral responses and device characteristics.

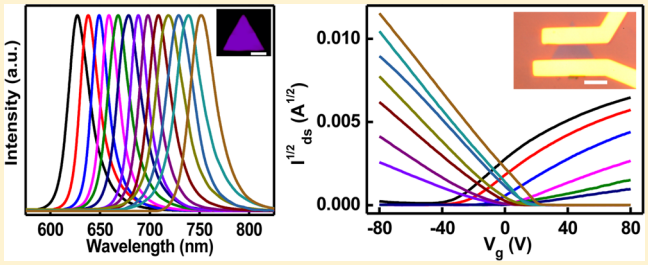

KEYWORDS: *Layered materials, transition metal dichalcogenide, semiconductor alloy, band gap engineering, field effect transistor, threshold voltage*

Two-dimensional (2D) layered materials are emerging as an exciting class of material system that has the potential to enable breakthroughs in fundamental materials science and create totally new technologies.[1−13] In general, a large family of layered materials (e.g., MoS_2, WS_2, $NbSe_2$, and Bi_2Te_3) in which the atomic layers are weakly bonded together by van der Waals interactions can be isolated into single- or few-layer nanosheets, allowing access to a wide range of physical properties at the atomic scale, such as metallic, semimetallic, semiconducting, insulating, topological insulating, superconducting, and thermoelectric properties.[1−3,14−20] In particular, the layered transition metal dichalcogenides (TMDs) (e.g., MoS_2, WSe_2) represent a large family of layered materials, many of which exhibit a tunable band gap that transits from an indirect band gap in bulk crystals to a direct band gap in monolayer nanosheets.[15−17,21,22] These 2D nanosheets typically have well-defined crystalline structure with few surface dangling bonds that traditionally plague conventional semiconductor nanostructures. These 2D-TMDs have thus emerged as an exciting class of atomically thin semiconductors for a new generation of electronic, optoelectronic, and valleytronic devices, as well as ultrasensitive sensors.[15,17,23−43]

Recent studies have demonstrated the exciting potentials of these 2D semiconductors, including the creation of atomically thin transistors that function in the gigahertz regime and entirely new types of heterostructure devices.[23,24,27,28,31,32,36,37,44] However, the studies to date are largely based on small flakes obtained from mechanical exfoliation. Rational chemical synthesis of 2D-TMDs and their heterostructures represents a significant challenge and has motivated

Received: September 10, 2015
Revised: November 1, 2015
Published: December 3, 2015

DOI: 10.1021/acs.nanolett.5b03662
Nano Lett. 2016, 16, 264−269

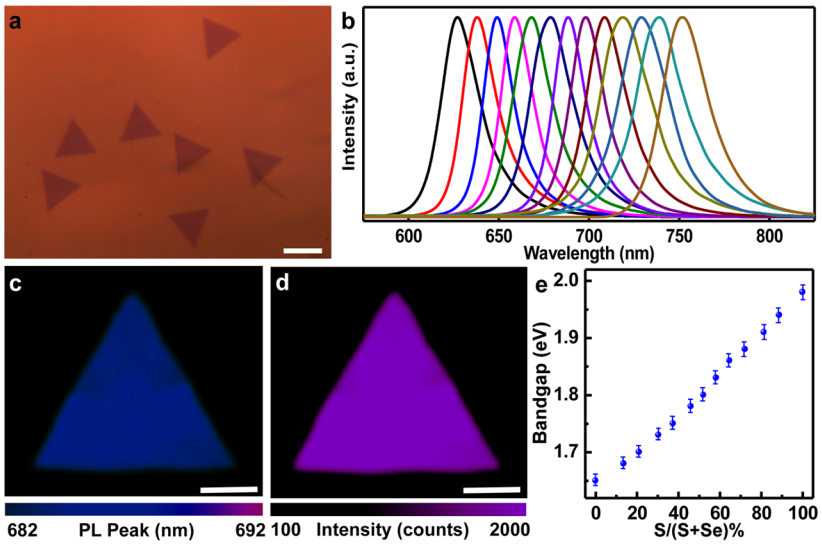

Figure 1. Bandgap engineering of $WS_{2x}WSe_{2-2x}$ nanosheets. (a) Optical microscopy image of typical $WS_{2x}Se_{2-2x}$ nanosheets (x = 0.454; scale bar = 20 μm. (b) Photoluminescence spectra of a series of composition tunable $WS_{2x}Se_{2-2x}$ monolayer nanosheets. (c) Photoluminescence peak position mapping of one typical $WS_{2x}Se_{2-2x}$ nanosheets (x = 0.522; scale bar = 10 μm). (d) Photoluminescence intensity mapping of the same $WS_{2x}Se_{2-2x}$ nanosheets (x = 0.522; mapping peak = 687.5 nm; scale bar = 10 μm). (e) Optical bandgap vs sulfur ratio in $WS_{2x}Se_{2-2x}$ nanosheets.

considerable efforts worldwide.[1,2,14,16,25,28,45−54] To explore the full potential of 2D-TMDs requires a precise control of their chemical compositions, physical dimensions, and hence the electronic and optical properties. For example, to design optoelectronic devices with desired spectral responses requires semiconductors with tunable band gaps.[24,27,30,31] Creating semiconductor alloys with variable chemical compositions is an effective strategy for the band gap engineering of bulk or thin film semiconductors. Using a similar strategy, a series of 2D-TMD alloy nanosheets have been recently prepared with tunable band gaps and optical properties.[45,48,55−66] The electronic properties of such alloy nanosheets are, however, rarely systematically explored to date.

In addition to band gap engineering, intentionally introducing a controllable number of impurity elements (~10^{16}−10^{19}/cm^3) into the bulk semiconductor lattice represents another key strategy to control the electronic properties of semiconductors. The impurity doping largely dictates the charge carrier type and carrier concentration in traditional semiconductors, and is central for creating functional electronic and optoelectronic devices. However, the controllable impurity doping in atomically thin 2D-TMD crystals represents a considerable challenge, and the systematic control of charge carrier type and concentration has not been achieved to date.[67−71] Recent studies indicate that the naturally grown WS_2 nanosheets on SiO_2/Si substrate mainly exhibit n-type semiconductor characteristics, while naturally grown WSe_2 nanosheets on SiO_2/Si substrate are mostly p-type semiconductors.[16,25,72] Therefore, it offers a plausible pathway to control the carrier type and electronic properties of such 2D nanosheets by creating a mixing alloy of WS_2 and WSe_2 with tunable chemical compositions. Here we report the synthesis of $WS_{2x}Se_{2-2x}$ alloy nanosheets with composition tunable optical and electronic properties.

The chemical vapor deposition (CVD) process has been recently developed for the growth of atomically thin 2D-TMDs on different substrate including SiO_2/Si, in which the target TMD vapor is generated by thermally evaporating the selected solid source.[14,16,50] This approach is rather versatile and has been applied for the synthesis of diverse 2D-TMD nanosheets (e.g., MoS_2, WS_2, $MoSe_2$, WSe_2) by simply switching the solid source. Additionally, it is also possible to produce the TMD alloy nanosheets by introducing multiple solid sources and mixing different TMD vapor-phase reactants in the aforementioned process.[25,45−47] In this study, to synthesize $WS_{2x}Se_{2-2x}$ nanosheets, the WS_2 and WSe_2 vapor-phase reactants are created by placing the respective solid material at different temperature in a home-built CVD system (Figure S1). The resulting vapor-phase reactants are mixed and transported downstream in argon carrier gas to produce $WS_{2x}Se_{2-2x}$ nanosheets on the SiO_2/Si substrates placed at the downstream end of the CVD system. The equilibrium partial pressure of WS_2 and WSe_2 and their ratio can be precisely controlled by systematically varying the temperature of the WS_2 and WSe_2 source to produce $WS_{2x}Se_{2-2x}$ nanosheets with fully tunable chemical compositions. (See Supporting Information for further experimental details.)

By systematically varying the growth parameters (see Supporting Information for details), we have produced a series of $WS_{2x}Se_{2-2x}$ nanosheets with continuously tunable alloy compositions on the 300 nm SiO_2/Si substrate. The resulting alloy nanosheets are typically monolayers with a well-defined triangular shape, as identified by optical contrast and atomic force microscopy studies (Figure 1a and Figure S2). To investigate the band gap modulation in the resulting alloy nanosheets, micro-photoluminescence (μ-PL) spectra were taken using a micro-Raman microscope and spectrometer excited by a 488 nm argon ion laser (power = 5 μW) in ambient condition. Photoluminescence studies demonstrate that all the monolayer samples display prominent emission with a single sharp peak with full width at half-maximum (fwhm) about 25 nm. The PL spectral peak positions are continuously tunable from 626.6 nm (nearly pure WS_2) to 751.9 nm (nearly pure WSe_2) depending on the exact synthetic conditions (Figure 1b). A spatially resolved mapping of the PL peak positions of an alloy nanosheet shows a rather small variation of the peak positions (<3 nm) across the entire triangular domain (Figure 1c), suggesting the spatially uniform chemical

DOI: 10.1021/acs.nanolett.5b03662
Nano Lett. 2016, 16, 264−269

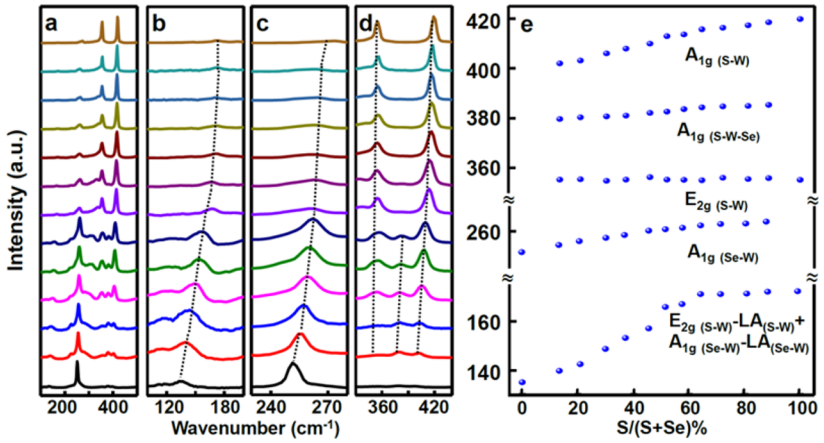

Figure 2. Evolution of Raman spectra in the $WS_{2x}Se_{2-2x}$ monolayer nanosheets as a function of chemical composition: (a) Full-range Raman spectra; (b) $E_{2g(S-W)}$-$LA_{(S-W)}$+$A_{1g(Se-W)}$-$LA_{(Se-W)}$ mode of the $WS_{2x}Se_{2-2x}$ nanosheets; (c) A_{1g} of Se−W mode; and (d) E_{2g} of S−W mode, A_{1g} of S−W−Se mode, and A_{1g} of S−W. (e) Raman spectra peak position shifts with increasing S atomic ratio for the five Raman modes.

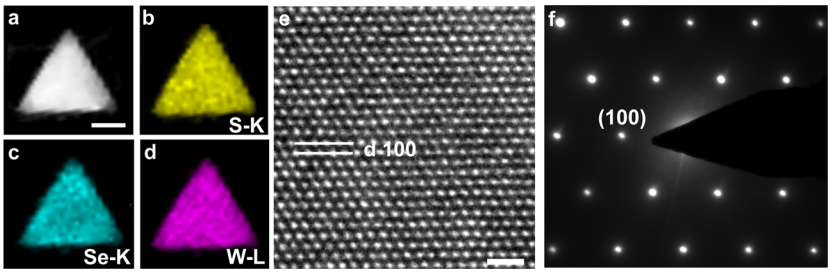

Figure 3. Composition and crystal structure analysis of the alloy nanosheet by TEM. (a) HAADF image of a small $WS_{2x}Se_{2-2x}$ domain (x = 0.573; scale bar = 500 nm). EDS mapping of the same triangular domain for S-K line (b), Se-K line (c), and W-L line (d). (e) High-resolution TEM image of a typical $WS_{2x}Se_{2-2x}$ nanosheet (x = 0.796; scale bar = 1 nm). (f) SAED pattern of a $WS_{2x}Se_{2-2x}$ nanosheet along the zone axis of [0001].

composition in the resulting nanosheets. Furthermore, the spatially resolved mapping of the PL intensity also shows a highly uniform contrast (Figure 1d), demonstrating highly uniform optical properties and crystalline quality. To correlate the band gap energy with the composition of the alloy nanosheets, we have approximated the band gap (E_g) using the PL emission peak position ($E_g = hc/\lambda$, where h is Planck's constant, c is the speed of light, and λ is the wavelength of PL peak) and determined the composition using energy dispersive X-ray spectroscopy (EDS) elemental analysis. The plot of the band gap vs composition shows an apparent linear relationship (Figure 1e), as expected for the ternary semiconductor alloys: $E_g(x) = xE_{gWS2} + (1 - x)E_{gWSe2}$, where x is the S/(S+Se) ratio.[61] These studies clearly demonstrate that the band gap of the alloy nanosheets can be fully tuned all the way from pure WSe_2 to pure WS_2 by systematically controlling the growth conditions. This band gap tunability in the $WS_{2x}Se_{2-2x}$ alloy system can greatly enrich 2D material family and enable spectral tunability for selected optoelectronic applications.

To further investigate the structural evolution in the $WS_{2x}Se_{2-2x}$ alloy nanosheets, we have collected the Raman spectra from the same sample series used for PL studies. In general, the Raman spectra display five main modes for most $WS_{2x}Se_{2-2x}$ nanosheets (Figure 2a), which can be assigned to $A_{1g(S-W)}$ mode (401.9−419.7 cm^{-1}), $A_{1g(Se-W)}$ mode (251.6−264.7 cm^{-1}), $A_{1g(S-W-Se)}$ mode (379.5−385.2 cm^{-1}), $E_{2g(S-W)}$ mode (~354.7−355.9 cm^{-1}), and $E_{2g(S-W)}$-$LA_{(S-W)}$+$A_{1g(Se-W)}$-$LA_{(Se-W)}$ mode (135.2−172.5 cm^{-1}). The normalized Raman spectra of the $WS_{2x}Se_{2-2x}$ nanosheets with modulated compositions show a clear peak position shift and relative intensity evolution for the A_{1g} mode (Figure 2e). The $A_{1g(S-W)}$ mode shows a strong resonance at 401.9 cm^{-1} for WSe_2-rich phase, that systematically shifts to the higher frequency (up to 419.7 cm^{-1}) with increasing intensity as the sulfur ratio increases; Similarly, the $A_{1g(Se-W)}$ mode follows the same trend and changes from a strong resonance at 251.6 cm^{-1} in pure WSe_2 phase to 264.7 cm^{-1} in WS_2-rich phase. The $E_{2g(S-W)}$-$LA_{(S-W)}$+$A_{1g(Se-W)}$-$LA_{(Se-W)}$ mode, i.e., the superposition of $E_{2g(S-W)}$-$LA_{(S-W)}$ and $A_{1g(Se-W)}$-$LA_{(Se-W)}$, also showed a systematic shift from 135.2 cm^{-1} in the WSe_2-rich phase to 172.5 cm^{-1} in the WS_2-rich phase, which matches well with the individual peak evolution of $E_{2g(S-W)}$ and $A_{1g(Se-W)}$ and is unique for $WS_{2x}Se_{2-2x}$ alloy nanosheets. Additionally, another extra alloy peak, the $A_{1g(S-W-Se)}$ mode, can also be observed in the $WS_{2x}Se_{2-2x}$ alloy nanosheets, with the resonance frequency shifting from 379.5 cm^{-1} in WSe_2-rich phase to 385.2 cm^{-1} in WS_2-rich phase. It is also interesting to note that $E_{2g(S-W)}$ mode remains at nearly the same frequency, with less than 1.2 cm^{-1} difference across the entire composition modulation range. There appears to be little contribution from the $E_{2g(Se-W)}$ mode, which could be attributed to very weak $E_{2g(Se-W)}$ mode and its weak coupling with the strong $E_{2g(S-W)}$ mode. The systematic Raman shifts further confirm the expected structural and compositional evolution in the $WS_{2x}Se_{2-2x}$ alloy nanosheets.

To further probe the microstructure of $WS_{2x}WSe_{2-2x}$ alloy nanosheets, transmission electron microscopy (TEM) studies, including energy-dispersive X-ray spectroscopy (EDS), high-resolution TEM (HRTEM) imaging, and selected area electron diffraction (SAED) (Figure 3), were employed for crystal structure and composition analyses. Figure 3a shows a low-

DOI: 10.1021/acs.nanolett.5b03662
Nano Lett. 2016, 16, 264−269

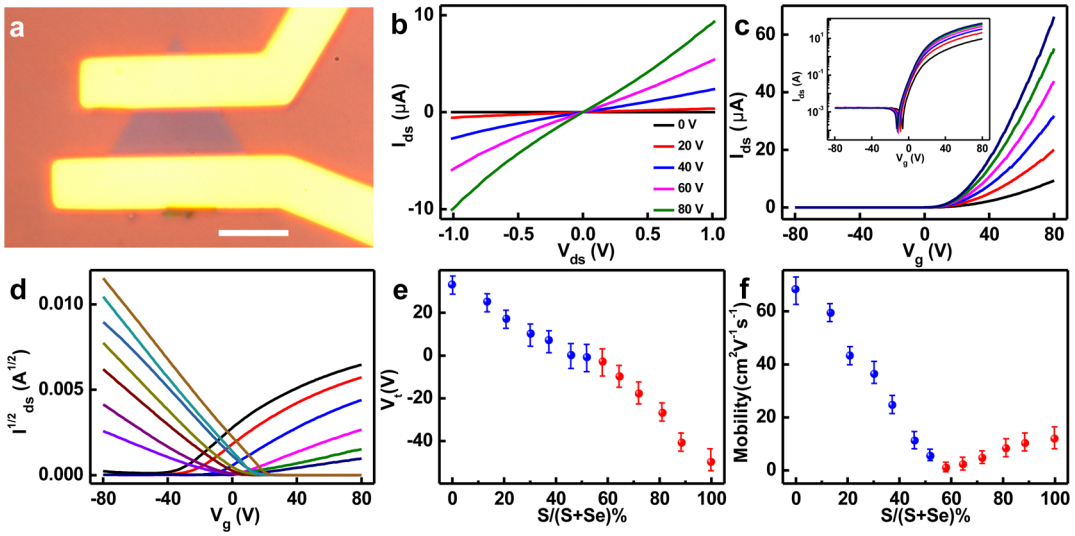

Figure 4. Electrical transport properties of $WS_{2x}Se_{2-2x}$ alloy nanosheets. (a) Optical microscopy image of a typical back-gated field effect transistor made of a $WS_{2x}Se_{2-2x}$ nanosheet (scale bar = 5 μm). (b) Output characteristics of a $WS_{2x}Se_{2-2x}$ nanosheet transistor (x = 0.813; gate voltage changing from 0 to 80 V in 20 V steps). (c) Transfer characteristics of the same transistor (source−drain bias changing from 0.5 to 3.0 V in 0.5 V steps); inset, log plot of I_{ds}−V_g curve. (d) Transfer characteristics ($I_d^{1/2}$−V_g plot) of $WS_{2x}Se_{2-2x}$ nanosheet transistors with different S atomic ratios from nearly pure WSe_2 (brown curve) to nearly pure WS_2 (black curve). (e) Alloy nanosheet transistor threshold voltage (V_t) vs S atomic ratio, with the blue dots highlighting the p-type behavior in WSe_2-rich alloys and red dots highlighting n-type behavior in WS_2-rich alloys. (f) Field effect mobility vs S atomic ratio relationship in $WS_{2x}Se_{2-2x}$ alloy nanosheets, with the blue dots representing the hole mobility in WSe_2-rich alloys and red dots representing electron mobility in WS_2-rich alloys.

magnification high-angle annular dark-field (HAADF) image of a $WS_{2x}Se_{2-2x}$ nanosheet. The spatially resolved EDS elemental mapping of the S, Se, and W elements shows relatively uniform distribution across a triangular domain, indicating composition uniformity throughout the entire domain (Figure 3b−d). The HRTEM image showed the well-resolved lattice fringe along (100) plane with no obvious defects, confirming the highly crystalline quality of the alloy nanosheets (Figure 3e). The selected-area electron diffraction (SAED) taken along the [0001] zone axis displays a single set of diffraction spots with 6-fold symmetry, further confirming the single-crystal quality of the alloy nanosheets (Figure 3f). A systematic analysis of a series of SAED patterns of a series of selected alloy samples shows that the lattice constant can be continuously tuned from 2.84 Å in nearly pure WSe_2 to 2.72 Å in nearly pure WS_2 (Figure S3), further confirming the successful alloy formation.

To probe the composition modulation of the electronic properties of the $WS_{2x}Se_{2-2x}$ alloy nanosheets, we have studied the electrical transport properties of $WS_{2x}Se_{2-2x}$ nanosheets using the back-gated field effect transistors (FETs). The back-gated nanohseet FETs are fabricated on 300 nm SiO_2/Si substrate (Figure 4a). In general, a single triangular domain is used as the transistor channel with a channel length around 5 μm. The source and drain electrodes are defined by using electron beam lithography and metallized by using electron beam evaporation (10 nm Ti/50 nm Au for S-rich alloys, and 50 nm Au for Se-rich alloys). The SiO_2/Si substrate is used as the back gate with the 300 nm SiO_2 as the gate dielectrics. The standard transistor measurements were conducted under ambient condition to derive the conductivity, on−off ratio, threshold voltage, and carrier type and mobility. To ensure consistency, 5−10 devices are fabricated from each sample to evaluate their electrical properties.

The output characteristics (the source−drain current (I_{sd}) vs source−drain voltage (V_{sd}) at varying back gate voltages) of a typical $WS_{2x}Se_{2-2x}$ nanosheet (x = 0.813) FET show nearly linear relationship (Figure 4b), indicating an Ohmic contact was achieved at the source−drain contacts. The current amplitude increases with increasingly positive gate voltage, suggesting an n-type semiconductor behavior. The transfer characteristics (I_{sd} vs gate voltage (V_g)) show that an on−off ratio of 10^5−10^8 can be achieved for most devices (Figure 4c and inset, and Figure S4). The electrical transport studies of the nanosheet devices with different alloy compositions show a systematic shift in carrier type, from p-type behavior in the WSe_2-rich phase to n-type semiconductors in the WS_2-rich phase, and a consistent shift of the threshold voltages as the composition is changed (Figure S5).

The evolution of electrical properties and FET threshold voltages can be more clearly seen from an $I_{sd}^{1/2}$−V_g plot under a source−drain bias of 3 V for the nanosheets with increasing sulfur atomic ratio from nearly pure WSe_2 (brown curve) to nearly pure WS_2 (black curve, Figure 4d). For the WSe_2-rich alloys (~0−0.55 S atomic ratio), the FETs predominantly display p-type semiconductor properties, whereas for the WS_2-rich alloys (~0.55−1 S atomic ratio), the n-type semiconductor properties are mainly observed. Additionally, it is noted that, for the intermediate alloy region (0.40−0.65 S atomic ratio), several devices showed weak ambipolar behavior (Figure S4). For WSe_2-rich alloys, the devices are normally "on" with a highest threshold voltage (V_t) of +33 V observed in the nearly pure WSe_2 nanosheets, suggesting relatively high hole-concentration. The extracted average positive threshold voltage of the alloy samples decreases with the decreasing selenium ratio, suggesting a reducing number of holes in the nanosheet transistors; Similarly for the WS_2-rich alloys, V_t = −50 V is observed for the nearly pure WS_2 sample, indicating the intrinsically n-type doping behavior. The negative threshold voltage also decreases with the decreasing sulfur ratio, signifying the decreasing electron carriers in the nanosheets with lower S ratio (Figure 4e). Overall, the WSe_2-rich alloys show highly p-type behavior, that gradually shifts to the lightly doped p-type

DOI: 10.1021/acs.nanolett.5b03662
Nano Lett. 2016, 16, 264−269

semiconductors as the Se ratio is decreased, and then switches to an n-type semiconductor character as the Se ratio is further decreased in the WS_2-rich alloys. The derived hole mobility dropped from 68.2 to 5.3 $cm^2\ V^{-1}\ s^{-1}$ as the Se-ratio is decreased in the Se-rich side. The electron mobility in S-rich alloys shows a similar trend, starting from a relatively high value of 11.8 $cm^2\ V^{-1}\ s^{-1}$ in the nearly pure WS_2, and decreasing to 0.9 $cm^2\ V^{-1}\ s^{-1}$ in the increasingly alloying samples. The mobility values achieved in the Se-rich and S-rich end samples are comparable to the best-reported mobility values for pure WSe_2 and WS_2 samples. The relative low mobility for intermediate alloyed $WS_{2x}Se_{2-2x}$ nanosheets ($0.30 < x < 0.80$) may be attributed partly to higher contact resistance due to lower doping concentration, and partly to the increased ionized impurity scattering and alloy scattering in the alloy sample, which is commonly observed in group III−V alloy semiconductors.[73] Our electrical transport studies clearly demonstrate that the carrier type and threshold voltages of the alloy nanohseet transistors can be systematically tuned by varying the alloy composition. We recognize that both the intrinsic doping (dominated by impurities, vacancies) and contact doping (dominated by band alignments) could affect the electrical transport characteristics of the alloy nanosheet transistors, and complete decoupling of these two doping effects is difficult. Further investigation of the electronic property evolution in the alloy nanosheets would be an interesting topic in future studies.

In summary, we have shown that $WS_{2x}Se_{2-2x}$ alloy nanosheets with fully tunable chemical compositions can be successfully grown on SiO_2/Si substrate by controlling the relative ratio of WS_2 and WSe_2 vapor in a home-built CVD system. Micro-photoluminescence and micro-Raman studies showed a systematic shift of PL peak position and the Raman resonance frequencies, indicating successful chemical and structural modulation and band gap engineering. TEM studies confirm single-crystalline structure with uniform alloy. Electrical transport studies further reveal a systematic modulation of the electronic properties, including the carrier type, threshold voltage, and mobility, as the alloy composition is changed. The successful growth of $WS_{2x}Se_{2-2x}$ nanosheets with tunable band gaps and electrical properties will greatly enrich the TMD material family, and could empower a great deal of flexibility in designing atomically thin electronics and optoelectronics with tailored device characteristics.

■ ASSOCIATED CONTENT

Supporting Information

The Supporting Information is available free of charge on the ACS Publications website at DOI: 10.1021/acs.nanolett.5b03662.

Experimental details and experimental setup, atomic force microscopy image, lattice constant analysis, and additional electrical characterization data of the alloy nanosheets (PDF)

■ AUTHOR INFORMATION

Corresponding Authors

* E-mail: rqyu@hnu.edu.cn.
* E-mail: xduan@chem.ucla.edu.

Author Contributions

⊗X.D. and C.W. contributed equally to this work.

Notes

The authors declare no competing financial interest.

■ ACKNOWLEDGMENTS

The effort at Hunan University (synthesis and partial optical characterizations) was supported by NSFC 61528403, and the effort at UCLA (characterizations) was supported by NSF DMR1508144.

■ REFERENCES

(1) Chhowalla, M.; Shin, H. S.; Eda, G.; Li, L. J.; Loh, K. P.; Zhang, H. *Nat. Chem.* **2013**, *5* (4), 263−275.

(2) Coleman, J. N.; Lotya, M.; O'Neill, A.; Bergin, S. D.; King, P. J.; Khan, U.; Young, K.; Gaucher, A.; De, S.; Smith, R. J.; Shvets, I. V.; Arora, S. K.; Stanton, G.; Kim, H. Y.; Lee, K.; Kim, G. T.; Duesberg, G. S.; Hallam, T.; Boland, J. J.; Wang, J. J.; Donegan, J. F.; Grunlan, J. C.; Moriarty, G.; Shmeliov, A.; Nicholls, R. J.; Perkins, J. M.; Grieveson, E. M.; Theuwissen, K.; McComb, D. W.; Nellist, P. D.; Nicolosi, V. *Science* **2011**, *331* (6017), 568−571.

(3) Novoselov, K. S.; Jiang, D.; Schedin, F.; Booth, T. J.; Khotkevich, V. V.; Morozov, S. V.; Geim, A. K. *Proc. Natl. Acad. Sci. U. S. A.* **2005**, *102* (30), 10451−10453.

(4) Butler, S. Z.; Hollen, S. M.; Cao, L. Y.; Cui, Y.; Gupta, J. A.; Gutierrez, H. R.; Heinz, T. F.; Hong, S. S.; Huang, J. X.; Ismach, A. F.; Johnston-Halperin, E.; Kuno, M.; Plashnitsa, V. V.; Robinson, R. D.; Ruoff, R. S.; Salahuddin, S.; Shan, J.; Shi, L.; Spencer, M. G.; Terrones, M.; Windl, W.; Goldberger, J. E. *ACS Nano* **2013**, *7* (4), 2898−2926.

(5) Huang, X.; Zeng, Z. Y.; Zhang, H. *Chem. Soc. Rev.* **2013**, *42* (5), 1934−1946.

(6) Zhang, H. *ACS Nano* **2015**, *9* (10), 9451−94659.

(7) Kuc, A.; Heine, T.; Kis, A. *MRS Bull.* **2015**, *40* (07), 577−584.

(8) Cao, L. *MRS Bull.* **2015**, *40* (07), 592−599.

(9) Shi, Y.; Zhang, H.; Chang, W.-H.; Shin, H. S.; Li, L.-J. *MRS Bull.* **2015**, *40* (07), 566−576.

(10) Amin, B.; Singh, N.; Schwingenschlögl, U. *Phys. Rev. B: Condens. Matter Mater. Phys.* **2015**, *92* (7), 075439.

(11) Chia, X.; Eng, A. Y. S.; Ambrosi, A.; Tan, S. M.; Pumera, M. *Chem. Rev.* **2015**, *115* (21), 11941−11966.

(12) Schmidt, H.; Giustiniano, F.; Eda, G. *Chem. Soc. Rev.* **2015**, *44* (21), 7715−7736.

(13) Duan, X.; Wang, C.; Pan, A.; Yu, R.; Duan, X. *Chem. Soc. Rev.* **2015**, DOI: 10.1039/C5CS00507H.

(14) Liu, K. K.; Zhang, W. J.; Lee, Y. H.; Lin, Y. C.; Chang, M. T.; Su, C.; Chang, C. S.; Li, H.; Shi, Y. M.; Zhang, H.; Lai, C. S.; Li, L. J. *Nano Lett.* **2012**, *12* (3), 1538−1544.

(15) Mak, K. F.; Lee, C.; Hone, J.; Shan, J.; Heinz, T. F. *Phys. Rev. Lett.* **2010**, *105* (13), 136805.

(16) Zhou, H. L.; Wang, C.; Shaw, J. C.; Cheng, R.; Chen, Y.; Huang, X. Q.; Liu, Y.; Weiss, N. O.; Lin, Z. Y.; Huang, Y.; Duan, X. F. *Nano Lett.* **2015**, *15* (1), 709−713.

(17) Wang, Q. H.; Kalantar-Zadeh, K.; Kis, A.; Coleman, J. N.; Strano, M. S. *Nat. Nanotechnol.* **2012**, *7* (11), 699−712.

(18) Chhowalla, M.; Liu, Z. F.; Zhang, H. *Chem. Soc. Rev.* **2015**, *44* (9), 2584−2586.

(19) Dang, W. H.; Peng, H. L.; Li, H.; Wang, P.; Liu, Z. F. *Nano Lett.* **2010**, *10* (8), 2870−2876.

(20) Guo, Y. F.; Lin, L.; Zhao, S. L.; Deng, B.; Chen, H. L.; Ma, B. J.; Wu, J. X.; Yin, J. B.; Liu, Z. F.; Peng, H. L. *Adv. Mater.* **2015**, *27* (29), 4315−4321.

(21) Splendiani, A.; Sun, L.; Zhang, Y. B.; Li, T. S.; Kim, J.; Chim, C. Y.; Galli, G.; Wang, F. *Nano Lett.* **2010**, *10* (4), 1271−1275.

(22) Eda, G.; Yamaguchi, H.; Voiry, D.; Fujita, T.; Chen, M. W.; Chhowalla, M. *Nano Lett.* **2011**, *11* (12), 5111−5116.

(23) Cheng, R.; Jiang, S.; Chen, Y.; Liu, Y.; Weiss, N.; Cheng, H. C.; Wu, H.; Huang, Y.; Duan, X. F. *Nat. Commun.* **2014**, *5*, 5143.

(24) Cheng, R.; Li, D. H.; Zhou, H. L.; Wang, C.; Yin, A. X.; Jiang, S.; Liu, Y.; Chen, Y.; Huang, Y.; Duan, X. F. *Nano Lett.* **2014**, *14* (10), 5590−5597.

DOI: 10.1021/acs.nanolett.5b03662
Nano Lett. 2016, 16, 264−269

(25) Duan, X. D.; Wang, C.; Shaw, J. C.; Cheng, R.; Chen, Y.; Li, H. L.; Wu, X. P.; Tang, Y.; Zhang, Q. L.; Pan, A. L.; Jiang, J. H.; Yu, R. Q.; Huang, Y.; Duan, X. F. *Nat. Nanotechnol.* **2014**, *9* (12), 1024−1030.
(26) Geim, A. K.; Grigorieva, I. V. *Nature* **2013**, *499* (7459), 419−425.
(27) Li, D. H.; Cheng, R.; Zhou, H. L.; Wang, C.; Yin, A. X.; Chen, Y.; Weiss, N. O.; Huang, Y.; Duan, X. F. *Nat. Commun.* **2015**, *6*, 7509.
(28) Li, M. Y.; Shi, Y. M.; Cheng, C. C.; Lu, L. S.; Lin, Y. C.; Tang, H. L.; Tsai, M. L.; Chu, C. W.; Wei, K. H.; He, J. H.; Chang, W. H.; Suenaga, K.; Li, L. J. *Science* **2015**, *349* (6247), 524−528.
(29) Liu, Y.; Wu, H.; Cheng, H.-C.; Yang, S.; Zhu, E.; He, Q.; Ding, M.; Li, D.; Guo, J.; Weiss, N. O.; Huang, Y.; Duan, X. *Nano Lett.* **2015**, *15* (5), 3030−3034.
(30) Lopez-Sanchez, O.; Lembke, D.; Kayci, M.; Radenovic, A.; Kis, A. *Nat. Nanotechnol.* **2013**, *8* (7), 497−501.
(31) Pospischil, A.; Furchi, M. M.; Mueller, T. *Nat. Nanotechnol.* **2014**, *9* (4), 257−261.
(32) Ross, J. S.; Klement, P.; Jones, A. M.; Ghimire, N. J.; Yan, J. Q.; Mandrus, D. G.; Taniguchi, T.; Watanabe, K.; Kitamura, K.; Yao, W.; Cobden, D. H.; Xu, X. D. *Nat. Nanotechnol.* **2014**, *9* (4), 268−272.
(33) Roy, K.; Padmanabhan, M.; Goswami, S.; Sai, T. P.; Ramalingam, G.; Raghavan, S.; Ghosh, A. *Nat. Nanotechnol.* **2013**, *8* (11), 826−830.
(34) Sie, E. J.; McIver, J.; Lee, Y. H.; Fu, L.; Kong, J.; Gedik, N. *Nat. Mater.* **2015**, *14* (3), 290−294.
(35) Wu, S. F.; Ross, J. S.; Liu, G. B.; Aivazian, G.; Jones, A.; Fei, Z. Y.; Zhu, W. G.; Xiao, D.; Yao, W.; Cobden, D.; Xu, X. D. *Nat. Phys.* **2013**, *9* (3), 149−153.
(36) Yu, W. J.; Li, Z.; Zhou, H. L.; Chen, Y.; Wang, Y.; Huang, Y.; Duan, X. F. *Nat. Mater.* **2013**, *12* (3), 246−252.
(37) Yu, W. J.; Liu, Y.; Zhou, H. L.; Yin, A. X.; Li, Z.; Huang, Y.; Duan, X. F. *Nat. Nanotechnol.* **2013**, *8* (12), 952−958.
(38) Mai, C.; Barrette, A.; Yu, Y. F.; Semenov, Y. G.; Kim, K. W.; Cao, L. Y.; Gundogdu, K. *Nano Lett.* **2014**, *14* (1), 202−206.
(39) Zou, X. M.; Wang, J. L.; Chiu, C. H.; Wu, Y.; Xiao, X. H.; Jiang, C. Z.; Wu, W. W.; Mai, L. Q.; Chen, T. S.; Li, J. C.; Ho, J. C.; Liao, L. *Adv. Mater.* **2014**, *26* (36), 6255−6261.
(40) Buscema, M.; Steele, G. A.; van der Zant, H. S. J.; Castellanos-Gomez, A. *Nano Res.* **2014**, *7* (4), 561−571.
(41) Li, H.; Wu, J.; Yin, Z.; Zhang, H. *Acc. Chem. Res.* **2014**, *47* (4), 1067−1075.
(42) Yin, Z.; Li, H.; Li, H.; Jiang, L.; Shi, Y.; Sun, Y.; Lu, G.; Zhang, Q.; Chen, X.; Zhang, H. *ACS Nano* **2012**, *6* (1), 74−80.
(43) Jiang, S.; Cheng, R.; Ng, R.; Huang, Y.; Duan, X. *Nano Res.* **2015**, *8* (1), 257−262.
(44) Zhang, W. J.; Chuu, C. P.; Huang, J. K.; Chen, C. H.; Tsai, M. L.; Chang, Y. H.; Liang, C. T.; Chen, Y. Z.; Chueh, Y. L.; He, J. H.; Chou, M. Y.; Li, L. J. *Sci. Rep.* **2014**, *4*, 3826.
(45) Li, H. L.; Duan, X. D.; Wu, X. P.; Zhuang, X. J.; Zhou, H.; Zhang, Q. L.; Zhu, X. L.; Hu, W.; Ren, P. Y.; Guo, P. F.; Ma, L.; Fan, X. P.; Wang, X. X.; Xu, J. Y.; Pan, A. L.; Duan, X. F. *J. Am. Chem. Soc.* **2014**, *136* (10), 3756−3759.
(46) Gong, Y. J.; Lin, J. H.; Wang, X. L.; Shi, G.; Lei, S. D.; Lin, Z.; Zou, X. L.; Ye, G. L.; Vajtai, R.; Yakobson, B. I.; Terrones, H.; Terrones, M.; Tay, B. K.; Lou, J.; Pantelides, S. T.; Liu, Z.; Zhou, W.; Ajayan, P. M. *Nat. Mater.* **2014**, *13* (12), 1135−1142.
(47) Huang, C. M.; Wu, S. F.; Sanchez, A. M.; Peters, J. J. P.; Beanland, R.; Ross, J. S.; Rivera, P.; Yao, W.; Cobden, D. H.; Xu, X. D. *Nat. Mater.* **2014**, *13* (12), 1096−1101.
(48) Li, H. L.; Zhang, Q. L.; Duan, X. D.; Wu, X. P.; Fan, X. P.; Zhu, X. L.; Zhuang, X. J.; Hu, W.; Zhou, H.; Pan, A. L.; Duan, X. F. *J. Am. Chem. Soc.* **2015**, *137* (16), 5284−5287.
(49) Schmidt, H.; Wang, S. F.; Chu, L. Q.; Toh, M.; Kumar, R.; Zhao, W. J.; Neto, A. H. C.; Martin, J.; Adam, S.; Ozyilmaz, B.; Eda, G. *Nano Lett.* **2014**, *14* (4), 1909−1913.
(50) Shaw, J. C.; Zhou, H. L.; Chen, Y.; Weiss, N. O.; Liu, Y.; Huang, Y.; Duan, X. F. *Nano Res.* **2014**, *7* (4), 511−517.
(51) Chen, Y.-Z.; Medina, H.; Su, T.-Y.; Li, J.-G.; Cheng, K.-Y.; Chiu, P.-W.; Chueh, Y.-L. *ACS Nano* **2015**, *9* (4), 4346−4353.
(52) Chen, J. Z.; Wu, X. J.; Yin, L. S.; Li, B.; Hong, X.; Fan, Z. X.; Chen, B.; Xue, C.; Zhang, H. *Angew. Chem., Int. Ed.* **2015**, *54* (4), 1210−1214.
(53) Tan, C.; Zhang, H. *J. Am. Chem. Soc.* **2015**, *137* (38), 12162−12174.
(54) Tan, C. L.; Zeng, Z. Y.; Huang, X.; Rui, X. H.; Wu, X. J.; Li, B.; Luo, Z. M.; Chen, J. Z.; Chen, B.; Yan, Q. Y.; Zhang, H. *Angew. Chem., Int. Ed.* **2015**, *54* (6), 1841−1845.
(55) Feng, Q.; Zhu, Y.; Hong, J.; Zhang, M.; Duan, W.; Mao, N.; Wu, J.; Xu, H.; Dong, F.; Lin, F.; Jin, C.; Wang, C.; Zhang, J.; Xie, L. *Adv. Mater.* **2014**, *26* (17), 2648−2653.
(56) Huang, Y. L.; Chen, Y. F.; Zhang, W. J.; Quek, S. Y.; Chen, C. H.; Li, L. J.; Hsu, W. T.; Chang, W. H.; Zheng, Y. J.; Chen, W.; Wee, A. T. S. *Nat. Commun.* **2015**, *6*, 6298.
(57) Zheng, S. J.; Sun, L. F.; Yin, T. T.; Dubrovkin, A. M.; Liu, F. C.; Liu, Z.; Shen, Z. X.; Fan, H. J. *Appl. Phys. Lett.* **2015**, *106* (6), 063113.
(58) Mouri, S.; Miyauchi, Y.; Matsuda, K. *Nano Lett.* **2013**, *13* (12), 5944−5948.
(59) Tongay, S.; Narang, D. S.; Kang, J.; Fan, W.; Ko, C. H.; Luce, A. V.; Wang, K. X.; Suh, J.; Patel, K. D.; Pathak, V. M.; Li, J. B.; Wu, J. Q. *Appl. Phys. Lett.* **2014**, *104* (1), 012101.
(60) Zhang, W.; Li, X.; Jiang, T.; Song, J.; Lin, Y.; Zhu, L.; Xu, X. *Nanoscale* **2015**, *7* (32), 13554−13560.
(61) Kang, J.; Tongay, S.; Li, J. B.; Wu, J. Q. *J. Appl. Phys.* **2013**, *113* (14), 143703.
(62) Song, J. G.; Ryu, G. H.; Lee, S. J.; Sim, S.; Lee, C. W.; Choi, T.; Jung, H.; Kim, Y.; Lee, Z.; Myoung, J. M.; Dussarrat, C.; Lansalot-Matras, C.; Park, J.; Choi, H.; Kim, H. *Nat. Commun.* **2015**, *6*, 7817.
(63) Su, S.-H.; Hsu, W.-T.; Hsu, C.-L.; Chen, C.-H.; Chiu, M.-H.; Lin, Y.-C.; Chang, W.-H.; Suenaga, K.; He, H., Jr.; Li, L.-J. *Front. Energy Res.* **2014**, *2*, 27.
(64) Fu, Q.; Yang, L.; Wang, W.; Han, A.; Huang, J.; Du, P.; Fan, Z.; Zhang, J.; Xiang, B. *Adv. Mater.* **2015**, *27* (32), 4732−4738.
(65) Gan, L.-Y.; Zhang, Q.; Zhao, Y.-J.; Cheng, Y.; Schwingenschlögl, U. *Sci. Rep.* **2014**, *4*, 6691.
(66) Klee, V.; Preciado, E.; Barroso, D.; Nguyen, A. E.; Lee, C.; Erickson, K. J.; Triplett, M.; Davis, B.; Lu, I. H.; Bobek, S.; McKinley, J.; Martinez, J. P.; Mann, J.; Talin, A. A.; Bartels, L.; Léonard, F. *Nano Lett.* **2015**, *15* (4), 2612−2619.
(67) Dolui, K.; Rungger, I.; Das Pemmaraju, C.; Sanvito, S. *Phys. Rev. B: Condens. Matter Mater. Phys.* **2013**, *88* (7), 075420.
(68) Fang, H.; Tosun, M.; Seol, G.; Chang, T. C.; Takei, K.; Guo, J.; Javey, A. *Nano Lett.* **2013**, *13* (5), 1991−1995.
(69) Fang, H.; Chuang, S.; Chang, T. C.; Takei, K.; Takahashi, T.; Javey, A. *Nano Lett.* **2012**, *12* (7), 3788−3792.
(70) Kiriya, D.; Tosun, M.; Zhao, P. D.; Kang, J. S.; Javey, A. *J. Am. Chem. Soc.* **2014**, *136* (22), 7853−7856.
(71) Suh, J.; Park, T. E.; Lin, D. Y.; Fu, D. Y.; Park, J.; Jung, H. J.; Chen, Y. B.; Ko, C.; Jang, C.; Sun, Y. H.; Sinclair, R.; Chang, J.; Tongay, S.; Wu, J. Q. *Nano Lett.* **2014**, *14* (12), 6976−6982.
(72) Zhang, Y.; Zhang, Y. F.; Ji, Q. Q.; Ju, J.; Yuan, H. T.; Shi, J. P.; Gao, T.; Ma, D. L.; Liu, M. X.; Chen, Y. B.; Song, X. J.; Hwang, H. Y.; Cui, Y.; Liu, Z. F. *ACS Nano* **2013**, *7* (10), 8963−8971.
(73) Adachi, S. *Physical Properties of III-V Semiconductor Compounds*; John Wiley & Sons, Inc.: New York, 1992.

DOI: 10.1021/acs.nanolett.5b03662
Nano Lett. 2016, 16, 264−269